ARTICLE

Epimers with distinct mechanical behaviours

Udaya B. Rao Khandavilli,[a] Aoife M. Buckley,[a] Anita R. Maguire,[b] Mangalampalli S. R. N. Kiran,[c] Upadrasta Ramamurty,[d,e] and Simon E. Lawrence,*[a]

Received 00th January 20xx,
Accepted 00th January 20xx

DOI: 10.1039/x0xx00000x

This study highlights the impact of relative stereochemistry in epimer compounds on their mechanical properties; the crystals of one series of esters are ductile and deform plastically upon bending, whereas the other series all brittle. Nanoindentation studies show that the hardness, *H*, and elastic moduli, *E*, of the brittle crystals are substantially larger than those of the ductile ones. For the brittle crystals *H* values range from 153(10) to 293(37) MPa, *E* from 2.85 (0.33) to 9.10(0.51) GPa, whereas for the ductile crystals *H* range from 76(2) to 125(11) MPa, and *E* from 1.40(0.36) and 2.75(0.06) GPa. These are rationalized by recourse to the distinct crystal structural features, especially in terms of interdigitation in the molecular planes in the brittle crystals and slip planes in the ductile crystals. The indentation fracture toughness, K_c, of the (2'S) crystals are higher than those typically reported for molecular crystals, due to the corrugated nature of their crystal packing which enhances the crack tortuosity. The K_c values are in the range 0.215 (0.08) to 0.278 (0.06) MPa $m^{½}$ and the brittleness index values are in the range 711(19) to 1053(50) $m^{-½}$.

Introduction

Molecular crystals with unique mechanical responses have significant potential for applications in pharmaceutical, electronic and optical device industries. They can also be utilized as artificial muscles, explosives, and smart nanomaterials.[1-11] Recently, there have been significant advances in developing a broad structure - mechanical property framework that has allowed well-known crystal engineering principles to be employed in the design of these emerging class of materials.[12-26] This was made possible due to the adaption of the nanoindentation technique, which is widely used for characterizing structural metals and alloys that are often only available in small volumes (as in thin films or wires), for quantitative assessment of the mechanical properties of molecular crystals. Such an assessment was not possible before, due to the relatively small size of single crystals of organic materials, which rendered them not amenable for conventional mechanical characterization. While a large body of data on mechanical properties of molecular crystals and a reasonable understanding of the connections between the structural features in them and the properties is now available;[18-26] there have been no reports of the mechanical properties of epimers, especially their distinct mechanical nature on the basis of the configuration at one stereogenic centre. In the context of the strong dependence of the biological activity of compounds used as drugs on precise stereochemical features, understanding the mechanical properties of diastereomers or epimers is of interest, in particular, in terms of impact on the mechanical processing steps utilized during formulation. Key questions concern whether there would be a systematic variation in the mechanical properties within such a series, and the impact of stereochemistry.

While performing initial qualitative mechanical tests (bending) on both epimers of the L-menthyl-substituted methyl esters **1a** and **1b**, each of which were enantiopure, we observed that one epimer (*R* at the 2' position) formed crystals that were plastically bendable, *i.e.* they are ductile, while the crystals of the other epimer (*S* at the 2' position) were brittle and fragmented upon some initial elastic deformation. Intriguingly, expanding the series to include the progressively larger Et, ^{i}Pr and ^{t}Bu ester moieties **2-4a/b** revealed that the distinct mechanical responses found in the methyl derivative **1a/b** were mirrored in these larger compounds, Fig. 1. To investigate this serendipitous discovery in more detail, we have performed nanoindentation studies on the major faces of the single crystals of each of the compounds in these series, in order to obtain quantitative information about their mechanical properties. The results of these experiments are discussed, in conjunction with the underlying structural features, to illuminate the reasons for the distinct mechanical

[a] *School of Chemistry, Analytical and Biological Chemistry Research Facility, Synthesis and Solid State Pharmaceutical Centre, University College Cork, College Road, Cork, Ireland.*
[b] *School of Chemistry and School of Pharmacy, Analytical and Biological Chemistry Research Facility, Synthesis and Solid State Pharmaceutical Centre, University College Cork, College Road, Cork, Ireland.*
[c] *Department of Physics and Nanotechnology, Faculty of Engineering and Technology, SRM Institute of Science and Technology, SRM Nagar, Kattankulathur, 603203, Kanchipuram, Chennai, India.*
[d] *School of Mechanical and Aerospace Engineering, Nanyang Technological University, Singapore 639798, Republic of Singapore.*
[e] *Institute of Materials Research and Engineering, Agency for Science, Technology and Research (A ⁎STAR), Singapore 138634*
† Electronic Supplementary Information (ESI) available: [Experimental procedures, and analytical data for new compounds, crystallographic and nanoindentation data]. See DOI: 10.1039/x0xx00000x

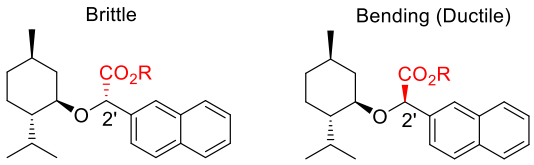

R = Me: (2'*S*)-Me **1a** R = Me: (2'*R*)-Me **1b**
Et: (2'*S*)-Et **2a** Et: (2'*R*)-Et **2b**
^{i}Pr: (2'*S*)-^{i}Pr **3a** ^{i}Pr: (2'*R*)-^{i}Pr **3b**
^{t}Bu: (2'*S*)-^{t}Bu **4a** ^{t}Bu: (2'*R*)-^{t}Bu **4b**

Fig. 1 The two epimeric series of substituted menthyloxy-2'-esters examined in this study.

responses of these two series of epimeric crystals.

Experimental

Materials and methods

The compounds utilized in this study were obtained from Sigma-Aldrich and used without further purification. Solvents were obtained from commercial sources and distilled before use.

Single crystal X-ray diffraction data were collected on a Bruker APEX II DUO diffractometer[27] using monochromatized Cu Kα (λ = 1.54178 Å) radiation. The APEX suite of programmes,[28] incorporating the SHELX suite of programs,[29] were used. The structures were solved using direct methods and refined by full-matrix least-squares on F^2. Crystallographic data are provided in Tables 1 and 2. Analysis was undertaken using PLATON.[30]

Powder X-ray diffraction (PXRD) data were collected on STOE STADI MP diffractometer with Cu $K\alpha_1$ radiation, and theoretical PXRD patterns were generated from the appropriate crystallographic information files.

^{1}H NMR spectra were recorded at 20 °C on a BRUKER AVANCE 300 MHz spectrometer using DMSO-d_6 as solvent. Chemical shifts are given in ppm relative to tetramethylsilane (TMS) as an internal standard. Coupling constants (J) are given in hertz (Hz).

Differential Scanning Calorimetry was undertaken on crystalline samples grown for single crystal analysis using a TA Instruments Q1000 instrument. Typically 2-6 mg of the sample was used in a non-hermetic aluminium pans and scanned from 30 to 200 °C at a heating rate of 10 °C min^{-1} under a continuously purged dry nitrogen atmosphere.

A Bruker Tensor ATR 37 spectrometer was used for Infrared Spectroscopy, using the OPUS 7.2 software (Bruker Optics). Samples were placed on a diamond probe attenuated total reflectance (ATR) crystal accessory, and overall 32 scans were collected for each sample at a resolution of 2 cm^{-1} over a wavenumber range of 425–4000 cm^{-1}.

Attachment energy calculations were calculated using an expanded version of the Habit[31] program within the Oscail software package.[32]

The nanoindentation experiments were performed on the largest faces of the crystals using a nanoindenter (Bruker's Hysitron Triboindenter, USA). The machine continuously monitors and records the load (*P*) and displacement (*h*) of the indenter with resolutions of 1 nN and 0.2 nm, respectively. A Berkovich diamond indenter (tip radius of ~100 nm) was used to indent the crystals. A loading and unloading rate of 0.6 mN s^{-1} and a hold time of 10 s at peak load were employed. A minimum of 10 indentations on each crystal were performed to get reliable and consistent data. The experiments were conducted in quasi-static (load-controlled) mode. The hardness, *H*, and elastic modulus, *E*, were estimated using the Oliver-Pharr method.[33] Pile-up height correction was taken care of while estimating these properties.[34] The indentation impressions were captured after unloading using the same Berkovich tip operating in the scanning mode. Indentation axis is normal to the major face in all cases.

For estimating the indentation fracture toughness, *Kc*, the following expression developed by Lawn and colleagues,[35-37] was used:

$$K_C = \xi\left(\frac{E}{H}\right)^{\frac{1}{2}}\left(\frac{P_{max}}{c^{\frac{3}{2}}}\right),$$

where *c* is the crack length, *E* is the elastic modulus, *H* is the hardness, P_{max} is the maximum load and ξ is an empirical constant that depends on the geometry of the indenter (0.016 for Berkovich indenter).[38] The brittleness index, BI, is the ratio of indentation hardness to fracture toughness:[35]

$$BI = \frac{H}{K_c}.$$

General Procedure for O-H insertion

Rhodium(II) acetate (0.017 mmol) was added in one portion to a stirring solution of (-)-menthol (17 mmol) and the appropriate α-diazo ester (18 mmol) in CH_2Cl_2 (70 mL). The solution was stirred for 2 h at room temperature and the reaction mixture was concentrated under reduced pressure to give the desired compound as a mixture of diastereomers. Purification of the crude product by column chromatography on silica gel employing hexane/ethyl acetate (98:2) as the eluent allowed partial fractionation of diastereomers but not complete separation. Sequential recrystallizations from acetonitrile gave either the (2'S) or (2'R) derivative as a single epimer in each case. Further details, including the synthetic route, are provided in the ESI†.

Results and discussion

Structural Studies.

Single crystal X-ray diffraction‡ of the brittle compounds revealed that for all four compounds the close proximity in space of the alkyl moiety of the ester to the isopropyl group on the menthyl substituent results in out of plane rotation of the isopropyl group, Fig. 2. For (2'*S*)-Me, **1a**, and (2'*S*)-Et, **2a**, there are no significant intermolecular interactions except for a short

Table 1 Crystallographic data for the brittle (2'*S*) compounds, **1a** – **4a**.

	1a	**2a**	**3a**	**4a**
Formula	$C_{23}H_{30}O_3$	$C_{24}H_{32}O_3$	$C_{25}H_{34}O_3$	$C_{26}H_{36}O_3$
MW	354.47	368.49	382.52	396.55
Crystal system	orthorhombic	orthorhombic	orthorhombic	monoclinic
Space group, *Z*	$P2_12_12_1$, 4	$P2_12_12_1$, 4	$P2_12_12_1$, 4	$P2_1$, 4
a, Å	6.4082(5)	6.64180(10)	7.0826(2)	8.8941(2)
b, Å	15.8900(13)	15.8771(3)	16.1438(4)	11.0810(3)
c, Å	20.4115(16)	20.7515(4)	20.5765(5)	25.5820(7)
α, deg	90	90	90	90
β, deg	90	90	90	93.0290(10)
γ, deg	90	90	90	90
V, Å^3	2078.4(3)	2188.30(7)	2352.72(11)	2517.72(11)
T, K	296	296	296	296
Total reflns.	20325	20478	11475	23966
Unique reflns.	3628	3775	4050	8567
R_{int}	0.0252	0.0598	0.0239	0.0328
Obs. reflns., $I > 2\sigma(I)$	3555	3662	3797	8170
R_1 [$I > 2\sigma(I)$]	0.0414	0.0405	0.0712	0.0875
wR_2 [all data]	0.1164	0.1174	0.2179	0.2544
Flack	0.03(4)	0.05(7)	0.13(5)	-0.01(4)

Table 2 Crystallographic data for the ductile (2'*R*) compounds, **1b** – **4b**.

	1b	**2b**	**3b**	**4b**
Formula	$C_{23}H_{30}O_3$	$C_{24}H_{32}O_3$	$C_{25}H_{34}O_3$	$C_{26}H_{36}O_3$
MW	354.47	368.49	382.52	396.55
Crystal system	monoclinic	orthorhombic	monoclinic	orthorhombic
Space group, *Z*	$P2_1$, 2	$P2_12_12_1$, 4	$P2_1$, 2	$P2_12_12_1$, 4
a, Å	5.4511(4)	5.3651(3)	5.3605(4)	5.6104(2)
b, Å	8.7712(5)	9.6939(5)	10.0888(8)	9.8196(4)
c, Å	21.3404(12)	42.693(3)	21.4700(16)	43.1042(17)
α, deg	90	90	90	90
β, deg	90.438(4)	90	97.129(5)	90
γ, deg	90	90	90	90
V, Å^3	1020.31(11)	2220.4(2)	1152.14(15)	2374.69(16)
T, K	296	296	296	296
Total reflns.	4724	9594	8797	14620
Unique reflns.	2613	3726	3444	3860
R_{int}	0.0382	0.0325	0.0490	0.0282
Obs. reflns., $I > 2\sigma(I)$	2376	3385	3069	3749
R_1 [$I > 2\sigma(I)$]	0.0496	0.0627	0.0607	0.0452
wR_2 [all data]	0.1539	0.1686	0.1650	0.1152
Flack	0.3(2)	0.28(13)	0.03(14)	0.19(6)

C-H···H-C contact involving the L-menthyl group, Fig. 2. In (2'*S*)-^{i}Pr, **3a**, the carbonyl group on the ester interacts with one hydrogen atom of the isopropyl group via weak C=O···H-C hydrogen bonding to generate a zig-zag arrangement network, whereas in (2'*S*)-^{t}Bu, **4a**, a hydrogen atom on the naphthyl ring interacts via C=O···H-C hydrogen bonding with the carbonyl ester, Fig. 3.

In contrast, for the ductile crystals, the alkyl substituent on the stereogenic carbon and the isopropyl group on the L-menthyl unit are not close to one another in space due to the altered relative stereochemistry at the 2′-position. The naphthyl groups exhibit C-H…π interactions in all four compounds, Fig. 4 & 5. Details of intermolecular contacts are in Table 3.

Each of the experimental PXRD patterns is in good agreement with the calculated pattern generated from the crystallographic files, attesting to the bulk homogeneity of the samples. Attachment energy calculations show reasonable agreement between the calculated and observed crystal morphologies and indicate that the lowest energy plane (001) is the slip plane for all the ductile crystals examined (ESI†).

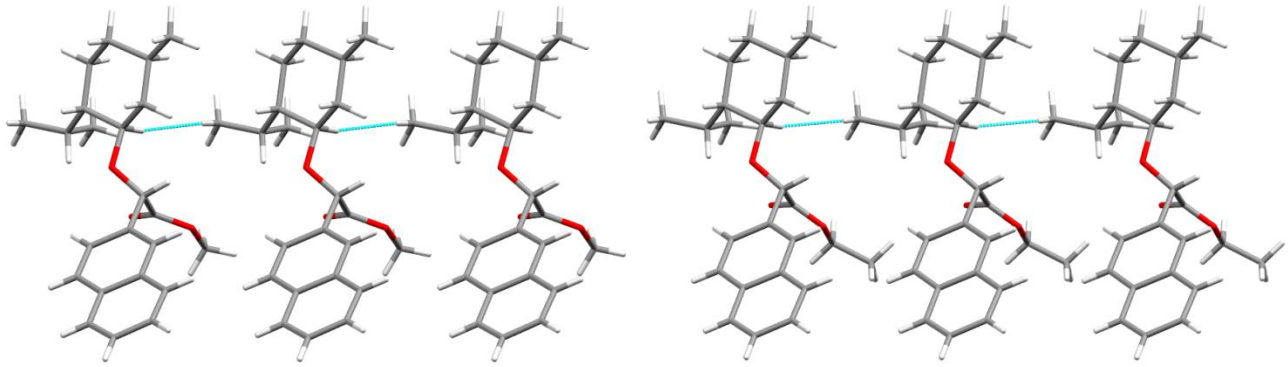

Fig. 2 The H···H close contacts in the brittle crystals: view down the *b*-axis for (2'S)-Me (**1a**), left, and view down the *b* axis for (2'S)-Et (**2a**), right. Minor disorder in **2a** omitted for clarity.

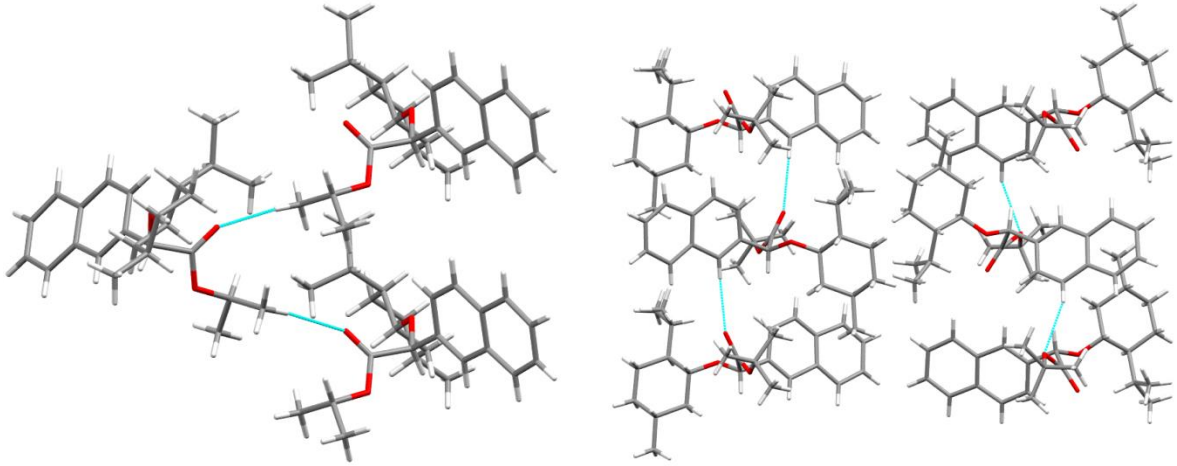

Fig. 3 Weak C-H…O interactions in (2'S)-^{i}Pr (**3a**) crystals viewed down the *c* axis, left. H…H close contacts in (2'S)-^{t}Bu (**4a**) viewed down the *a* axis, right. The two symmetry independent molecules in **4a** have close contacts only with their symmetry equivalent neighbours. This view of **4a**, coloured by symmetry equivalence, is in the ESI†. Minor disorder in one molecule of **4a** omitted for clarity.

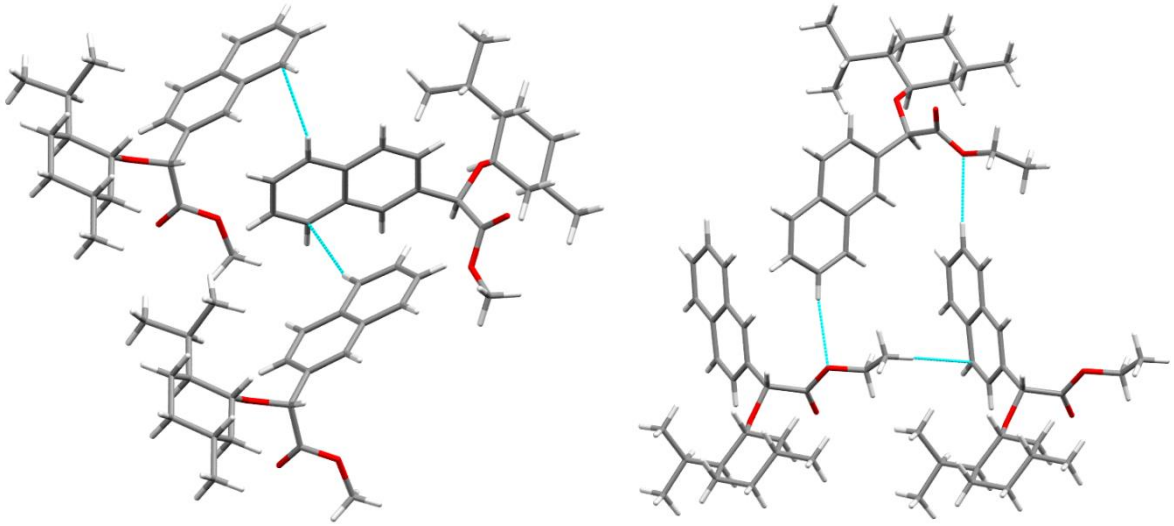

Fig. 4 View of the C-H…π contact in the ductile (2'S)-Me (**1b**), left, and C-H…O and C-H…π contacts in (2'S)-Et (**2b**), right.

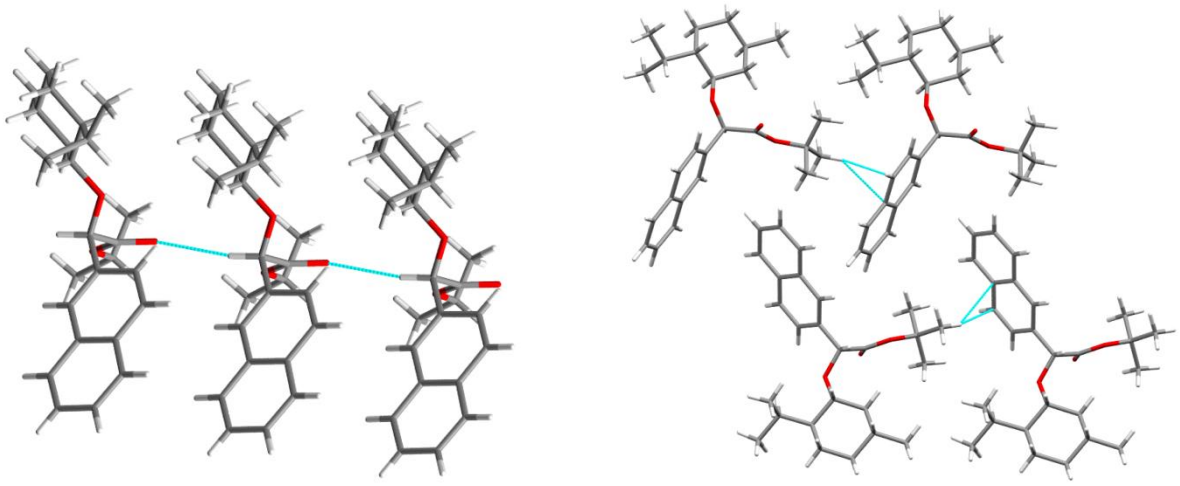

Fig. 5 Weak C-H…O interactions in (2'S)-^{i}Pr (**3b**) crystals viewed down the *b* axis, left, and C-H…π contact in (2'S)-^{t}Bu (**4b**), right.

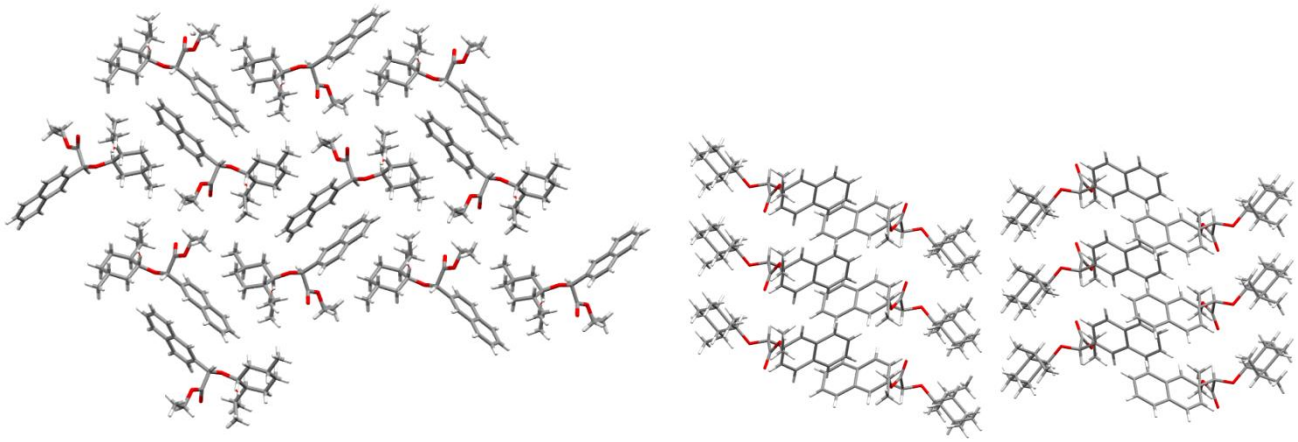

Fig. 6 Interdigitation in (2'*S*)-Et, **2a**, left. and the slip planes in (2'*R*)-Et, **2b**, right.

Table 3 Main intermolecular interactions or close contacts.[a]

Compound	At(I)	At(J)	Type	Distances / angles	ARU
1a	C4-H4	H12A	H···H close contact	2.11 Å, 141°	1+x, y, z
	C9-H9A	H19	H···H close contact	2.37 Å, 129°	½ +x, ½-y, 1-z
2a	C4-H4	H12B	H···H close contact	2.22 Å, 136°	-1+x, y, z
3a	C27-H27B	O24	C-H···O	2.59 Å, 174°	½+x, ½-y, 1-z
4a	C15-H15	O24	C-H···O	2.59 Å, 174°	1-x, -½+y, 1-z
	C52-H52	O55A [b]	C-H···O	2.59 Å, 148°	2-x, -½+y, 2-z
	C52-H52	O55B [b]	C-H···O	2.62 Å, 156°	2-x, -½+y, 2-z
1b	C18-H18	C21	C-H···π	2.85 Å, 158°	2-x, ½+y, 1-z
2b	C9 –H9A	O24	C-H···O	2.71 Å, 125°	1+x, y, z
	C18-H18	O25	C-H···O	2.69 Å, 169°	1-x, -½+y, $^{3}/_{2}$-z
	C19-H19	centroid [c]	C-H···π	2.91 Å, 157°	-x, -½+y, $^{3}/_{2}$-z
	C27-H27A	centroid [c]	C-H···π	2.84 Å, 167°	x, 1+y, z
3b	C12-H12	O14	C-H···O	2.62 Å, 166°	1+x, y, z
	C24-H24	centroid [d]	C-H···π	2.99 Å, 154°	1-x, -½+y, 1-z
4b	C28-H28B	centroid [c]	C-H···π	2.98 Å, 171°	x, 1+y, z

[a] based on PLATON[30] analysis
[b] disordered atom
[c] centroid of ring containing atoms C14, C15, C16, C21, C22, C23
[d] centroid of ring containing atoms C19, C20, C21, C26, C27, C28

As the steric demand of the ester moiety increases from Me to Et to ^{i}Pr to ^{t}Bu in both **1a**-**4a** and **1b**-**4b**, the relative conformation of the menthyl ring and the naphthyl unit adjusts to accommodate this increase (ESI†).

Prior studies on the mechanical properties of organic crystals have established that the long range shear sliding of crystallographic planes under the influence of the applied stress is responsible for the plasticity observed in molecular crystals.[19] A common way to achieve this is to have molecules connected by weak and strong interactions in mutually orthogonal arrangements. In addition, the presence/absence of active slip systems, the nature of molecular packing (interlocked *vs.* non-interlocked, *anti* or twisted conformation), and the presence/absence of strong interactions between slip planes play a significant role in determining the plastic flow in molecular crystals.[39]

The crystal structures for the two series of epimers provide a rationale for the observed distinct mechanical behaviour of the crystals, Fig. 6. For the (2'*S*) series, clear interdigitation of molecules can be seen, which prevents long-range molecular migration via slip and, hence, leads to the fracture of the crystals in a brittle manner after some initial elastic deformation. On the other hand, for the (2'*R*) series, a combination of the naphthyl groups forming π-stacked columns with van der Waals interactions between the hydrophobic alkyl groups leads to slip planes that are responsible for the ductile behaviour observed in these crystals.

Nanoindentation Studies.

Representative load, *P*, vs. depth of penetration, *h*, responses that were obtained using nanoindentation on the major faces, {100} planes of single crystals of all the compounds are displayed in Fig. 7. (The (2'*R*)-Me crystals were too soft and thin and, hence, were not amenable to nanoindentation.) For the maximum load (P_{max}) of 6 mN, the maximum penetration depths of the indenter (h_{max}) for crystals of the (2'*S*) epimers range between 0.8 and 1.2 μm. The corresponding range for the (2'*R*) crystals is larger, 1.3 to 1.8 μm, indicating that the (2'*S*) series are relatively harder and stiffer. The loading segments of the *P*-*h* responses of all the (2'*S*) epimers are serrated, due to the interdigitation in their packing, which offers cumulative resistance to the smooth penetration of the indenter into the crystal; instead microcracking of the crystals appears to be the mechanism for the stress relaxation. The pop-ins could be due to the intermittent cracking (either nucleation of corner cracks or stick-slip kind of advancement of an already nucleated crack). Indeed, images of the indenter imprints made on these crystals show microcracks along the edges of the indents, further confirming their brittle nature, Fig. 8 and ESI†.

In the case of 2'R series, though the {001} slip planes are expected to facilitate smooth deformation along <110>, the complex molecular packing together with the intermolecular contacts leads to intermittent plasticity. The observation of a significant amount of material pile-up around the indent edges

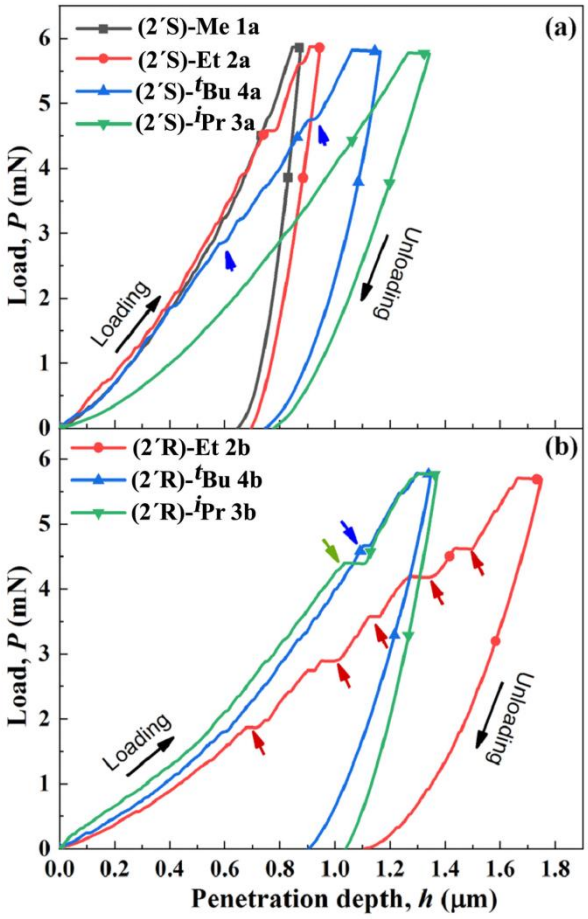

Fig. 7 Representative load vs. depth of penetration (P-h) responses obtained on the major faces of the single-crystals of (a) **1a**-**4a**, and (b) **2b**-**4b**.

made on these crystals further affirms their plastic nature.[40] The presence of cracks in the 2'*S* series with no pile-up of the deformed material, and the presence of pile-up without cracks in the 2'*R* series, are the most crucial shreds of evidence for differentiating them as brittle and ductile, respectively.

Values of the hardness (*H*) and the elastic modulus (*E*) are listed in Table 4. As expected from the *P*-*h* curves themselves, the (2'*S*) series of crystals, as a group, have considerably higher *H* and *E*, as compared to the (2'*R*) series of crystals. The higher *H* and *E* in the former is due to the hindrance to slip caused by the interdigitated structure.

Within each series of compounds, while the *H* and *E* values generally increase in the (2'S) series as the functional groups get progressively larger the opposite trend is seen in the (2'R) series. A possible reason for this could be that the methyl group in (2'S)-Me experiences less steric hindrance compared to the bulky functional groups that show higher steric (repulsion between the alkyl groups) hindrance. This, in turn, leads to tighter packing of the molecules, which enhances the crystals' resistance to elastic deformation. Similarly, (2'S)-*t*Bu shows less hardness as the planes in these crystals have more distance between the two layers due to the steric hindrance.

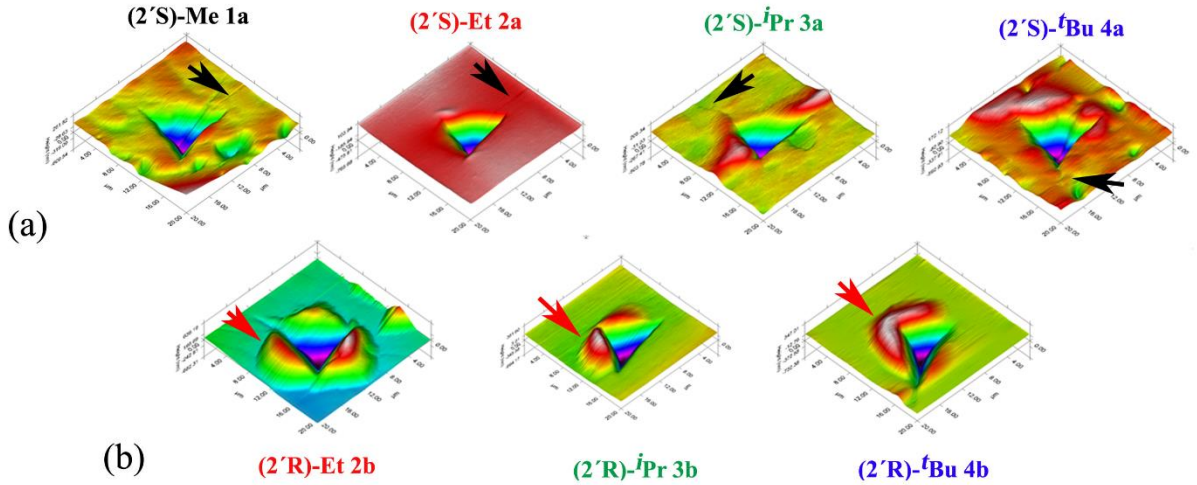

Fig. 8 The post-indent AFM scans (3D) of the residual indents of crystals mentioned in (a) 2'S series crystals, and (b) 2'R series crystals. The black arrows on (a) show cracks and red arrows on (b) show pile-up. The scan size of all the AFM images is 20 µm x 20 µm.

Table 4 Mechanical properties of the seven crystals examined using nanoindentation.

Compound	*H* (MPa)	*E* (GPa)	Crack Length (µm)	$(E/H)^{½}$	*Kc* (MPa $m^{½}$)	*BI* ($m^{-½}$)
(2'*S*)-Me, **1a**	293 ± 37	9.10 ± 0.51	7.1 ± 0.3	5.572	0.278 ± 0.06	1053 ± 50
(2'*S*)-Et, **2a**	222 ± 12	5.00 ± 0.33	8.0 ± 0.1	5.194	0.249 ± 0.09	891 ± 24
(2'*S*)-^{t}Bu, **4a**	162 ± 16	3.79 ± 0.12	9.2 ± 0.3	4.836	0.221 ± 0.05	733 ± 33
(2'*S*)-^{i}Pr, **3a**	153 ± 10	2.85 ± 0.33	7.1 ± 0.3	4.315	0.215 ± 0.08	711 ± 19
(2'*R*)-Et, **2b**	76 ± 2	1.40 ± 0.36	-----	4.291	–	–
(2'*R*)-^{i}Pr, **3b**	98 ± 12	1.92 ± 0.11	-----	4.426	–	–
(2'*R*)-^{t}Bu, **4b**	125 ± 11	2.75 ± 0.06	-----	4.690	–	–

Therefore, going from Me- to *i*Pr, H of the crystals decreases, and *vice versa* as the number of carbon atoms increases.

However, in the case of (2'R)-*t*Bu, the distance between adjacent naphthalene rings is more, hence higher *H* and *E* values are seen than in the (2'R)-*i*Pr and (2'R)-Et crystals.

Values of the indentation fracture toughness, *Kc*, could only be estimated for the (2'*S*) crystals; since no cracks were observed for the (2'*R*) crystals, their *Kc* could not be measured. In general, fracture in molecular crystals takes place either through cleavage at certain crystallographic planes (brittle crystals) or the maximum τ, where dislocation pile-up attains a critical density (ductile or plastic crystals).[15,41]

Values of *Kc* for the (2'*S*) crystals, listed in Table 4, show that they range between 0.21 and 0.28 MPa $m^{½}$. These are significantly higher than those reported for other molecular crystals, which are typically below 0.1 MPa $m^{½}$.[32] The relatively higher toughness in the present crystals may be due to the fact that there are no cleavage planes available in them, which would otherwise facilitate a low energy consuming path for crack propagation. Instead, the interdigitation of molecular planes along <010> makes the crack path tortuous. As is well known in the fracture mechanics field, when a crack gets deflected from its mode I path (or opening mode of fracturing), higher energy needs to be spent to keep the crack propagating, which, in turn, increase the fracture resistance of the solid.[42] The corrugated cracks observed support this hypothesis.

Amongst the four (2'*S*) compounds examined, the (2'*S*)-Me compound shows the highest fracture resistance. Interestingly, the *BI* of it is also the highest, although BI is inversely proportional to *Kc*,[35] and, hence, one would expect lower BI for the (2'*S*)-Me crystals. In this context, *Kc* depends on the *E*/*H* ratio,[35-37] which is much higher for the (2'*S*)-Me crystals; thus, higher *Kc* is observed. Since the difference in the hardness values is only double for (2'*S*)-Me to (2'*S*)-^{i}Pr compounds, both *BI* and *Kc* have followed the same trend.

The fact that the crystals of each of the esters display distinct mechanical behaviour (i.e. brittle vs ductile) for the two epimeric series is significant, indicative that this observation is not just a single unusual phenomenon, but reliably reoccurs across the series. This observation opens the possibility of alteration of the mechanical properties of crystals by design, through understanding the effect of stereochemistry on crystal structures, and, in turn, the mechanical response. The epimers possess exactly the same elements and the same covalent connectivity; simply switching the relative stereochemistry at a single carbon stereocenter results in this dramatic alteration of mechanical behaviour. As compounds used as APIs increasingly have multiple stereogenic centers this observation also has relevance to the physical properties of APIs.

Conclusions

Over 170 years after Louis Pasteur's historical observations concerning sodium ammonium tartrate intrigued the scientific community,[43] we have found a series of epimeric compounds, differing at only one stereogenic centre, whose crystals display distinct mechanical behaviour, ductile or brittle.

Conflicts of interest

There are no conflicts to declare.

Acknowledgements

The support of Science Foundation Ireland (12/RC/2275, 12/RC/2275_P2, 05/PICA/B802/EC07), the Irish Research Council (GOIPG/2013/225), the Science and Engineering Research Board, Govt. of India (CRG/2021/1902) and University College Cork 2013 Research Fund is gratefully acknowledged, as is Professor Patrick McArdle for assistance with the face-indexing and attachment energy calculations.

Notes and references

‡ CCDC numbers are 1990771-1990778.

1 P. Naumov, S. Chizhik, M. K. Panda, N. K. Nath, E. Boldyreva, *Chem. Rev.* 2015, **115**, 12440−12490.
2 A. Agarwal, E. Huang, S. Palecek, N. L. Abbott, *Adv. Mater*. 2008, **20**, 4804–4809.
3 M. Đaković, M. Borovina, M. Pisačić, C. B. Aakeröy, Z. Soldin, B.-M. Kukovec, I. Kodrin, *Angew. Chem. Int. Ed*. 2018, **57**, 14801−14805.
4 S. C. Sahoo, M. K. Panda, N. K.; Nath, P. Naumov, *J. Am. Chem. Soc.* 2013, **135**, 12241−12251.
5 Q. M. Zhang, H. Li, M. Poh, F. Xia, Z.-Y. Cheng, H. Xu, C. Huang, *Nature* 2002, **419**, 284−287.
6 Z. S. Yao, M. Mito, T. Kamachi, Y. Shiota. K. Yoshizawa, N. Azuma, Y. Miyazaki, K. Takahashi, K. Zhang, T. Nakanishi, S. Kang, S. Kanegawa, O. Sato, *Nat. Chem*. 2014, **6**, 1079−83.
7 S. Günes, H. Neugebauer, N. S. Sariciftci, *Chem. Rev*. 2007, **107**, 1324−1338.
8 N. Chandrasekhar, R. Chandrasekar, *Angew. Chem. Int. Ed*. 2012, **51**, 3556−3561.
9 E. M. Hunt, M. Jackson, Proceedings of the ASME 2010 International Mechanical Engineering Congress and Exposition. 2010, **12**, 55−60.
10 A. Mondal, B. Bhattacharya, S.Das, S. Bhunia, R. Chowdhury, S. Dey, C. M. Reddy, *Angew. Chem., Int. Ed.*, 2020, **59**, 2–12.
11 Z. Lu, Y. Zhang, H. Liu, K. Ye, W.Liu, H. Zhang, *Angew. Chem., Int. Ed.*, 2020, **59**, 4299-4303.
12 S. Das, A. Mondal, C. M. Reddy, *Chem. Soc. Rev*., 2020, **49**, 8878-8896.
13 G. R. Desiraju, *Crystal Engineering: The Design of Organic Solids.* Elsevier, Amsterdam, 1989.
14 G. R. Desiraju, *J. Am. Chem. Soc.* 2013, **135**, 9952−67.
15 S. Varughese, M. S. R. N. Kiran, U. Ramamurty, G. R. Desiraju, *Angew. Chem. Int. Ed.* 2013, **52**, 2701−2712.
16 S. Ghosh, A. Mondal, M. S. R. N. Kiran, U. Ramamurty, C. M. Reddy, *Cryst. Growth Des.* 2013, **13**, 4435−4441.
17 S. Varughese, M. S. R. N. Kiran, K. A. Solanko, A. D. Bond, U. Ramamurty, G. R. Desiraju, *Chem. Sci*. 2011, **2**, 2236−2242.
18 S. Saha, G. R. Desiraju, *Chem. Eur. J*. 2017, **23**, 4936−4943.
19 G. R. Krishna, R. Devarapalli, G. Lal, C. M. Reddy, *J. Am. Chem. Soc*. 2016, **138**, 13561-13567.
20 U. B. Rao Khandavilli, B. R. Bhogala, A. R. Maguire, S. E. Lawrence, *Chem. Commun*. 2017, **53**, 3381−3384.
21 C. M. Reddy, K. A. Padmanabhan, G. R. Desiraju,. *Cryst. Growth Des*. 2006, **6**, 2720−2731.
22 S. Saha, G. R. Desiraju, *Chem. Commun.* 2016, **52**, 7676−7679.
23 S. Saha, M. K. Mishra, C. M. Reddy, G. R. Desiraju, *Acc. Chem. Res.* 2018, **51**, 2957−2967.
24 M. K. Mishra, G. R. Desiraju , U. Ramamurty, and A. D. Bond, Angew. Chem. Int. Ed. 2014, 126, 13318-13321.
25 M. K. Mishra, U. Ramamurty and G. R. Desiraju, *J. Am. Chem. Soc.* 2015, 137, 5, 1794–1797.
26 M. K. Mishra, P. Sanphui, U. Ramamurty and G. R. Desiraju, *Cryst. Growth Des.* 2014, 14, 6, 3054–3061.
27 K. S. Eccles, S. P. Stokes, C. A. Daly, N. M. Barry, S. P. McSweeney, D. J. O'Neill, D. M. Kelly, W. B. Jennings, O. M. Ni Dhubhghaill, H. A. Moynihan, A. R. Maguire, S. E. Lawrence, *J. Appl. Crystallogr.* 2011, **44**, 213−215.
28 APEX2 v2009.3-0 Bruker AXS: Madison, WI, 2009.
29 G. M. Sheldrick, *Acta Crystallogr. C*. 2015, **71**, 3−8.
30 A. L. Spek, *Acta Crystallogr. E*. 2020, **76**, 1−11.
31 G. Clydesdale, R. Docherty, K. J. Roberts, *Comput. Phys. Commun.* 1991, **64**, 311−328.
32 P. McArdle, *J. Appl. Crystallogr*. 2017, **50**, 320−326.
33 W. C. Oliver, G. M. J. Pharr, *Mater. Res.*, 1992, **7**, 1564−1583.
34 M. Sowjanya, M. S. R. N. Kiran, *Crystals,* 2017, **7**, 324.
35 B. R. Lawn, D. B Marshall, *J. Am. Ceram. Soc*, 1979, **62**, 347−350.
36 B. R. Lawn, A.G. Evans, D. B. Marshall, *J. Am. Ceram. Soc*. 1980, **63**, 574–581.
37 G. R. Anstis, P. Chantikul, B. R. Lawn, D. B. Marshall, *J. Am. Ceram. Soc*., 1981, **64**, 533−538.
38 D.S. Harding, W.C. Oliver, G.M. Pharr, *Mater. Res. Soc. Symp. Proc*. 1995, **356**, 663−668.
39 M. K. Mishra, U. Ramamurty, G. R. Desiraju, *Curr. Opin. Solid State Mater. Sci*. 2016, **20**, 361−370.
40 M. S. R. N. Kiran, S. Varughese, U. Ramamurty, G.R. Desiraju, *CrystEngComm*, 2012, **14**, 2489–2493.
41 D. Olusanmi, K. J. Roberts, M. Ghadiri, Y. Ding, *Int. J. Pharm*. 2011, **411**, 49–63.
42 S. Suresh, Fatigue of Materials, 2nd Edition, Cambridge University Press, 1998.
43 H. D. Flack, *Acta Crystallogr. A*. 2009, **65**, 371–89.

